Amorphous and thin Si:H PV

ROB & LINDA COLLINS

Solar panels don't have to be conspicuous. The panels on this house are energy-efficient and fit neatly into the roof.

http://www.motherearthnews.com/Renewable-Energy/Thin-Film-Solar-Utility-Scale-PV-Power.aspx

Silicon, Si

Atomic number: 14
Atomic mass: 28.0855(3)
Natural abundance: 272000 ppm
Isotopes:
^{28}Si (27.9769265) - 92.23%
^{29}Si (28.9764947) - 4.67%
^{30}Si (29.9737702) - 3.10%

Derived from Latin *silex, silicis, meaning flint. Amorphous silicon was first prepared by J.J. Berzelius in 1824 by reducing K_2SiF_6 with molten potassium. The crystalline form, which the second allotrope form of the element, was first prepared by Deville in 1854. It was T. Thomson who named the element in 1831. He added the ending "on" in order to emphasize the analogy with boron and carbon.*

http://elements.etacude.com/Si.php

Advantages of a-Si: Has a direct bandgap, ~100x more absorption than c-Si
in visible range, 1 μm thick layer of a-Si:H absorbs 90% of solar energy
Can be deposited at low temperatures (<300 °C)
Can be deposited on inexpensive substrates (glass, stainless steel)
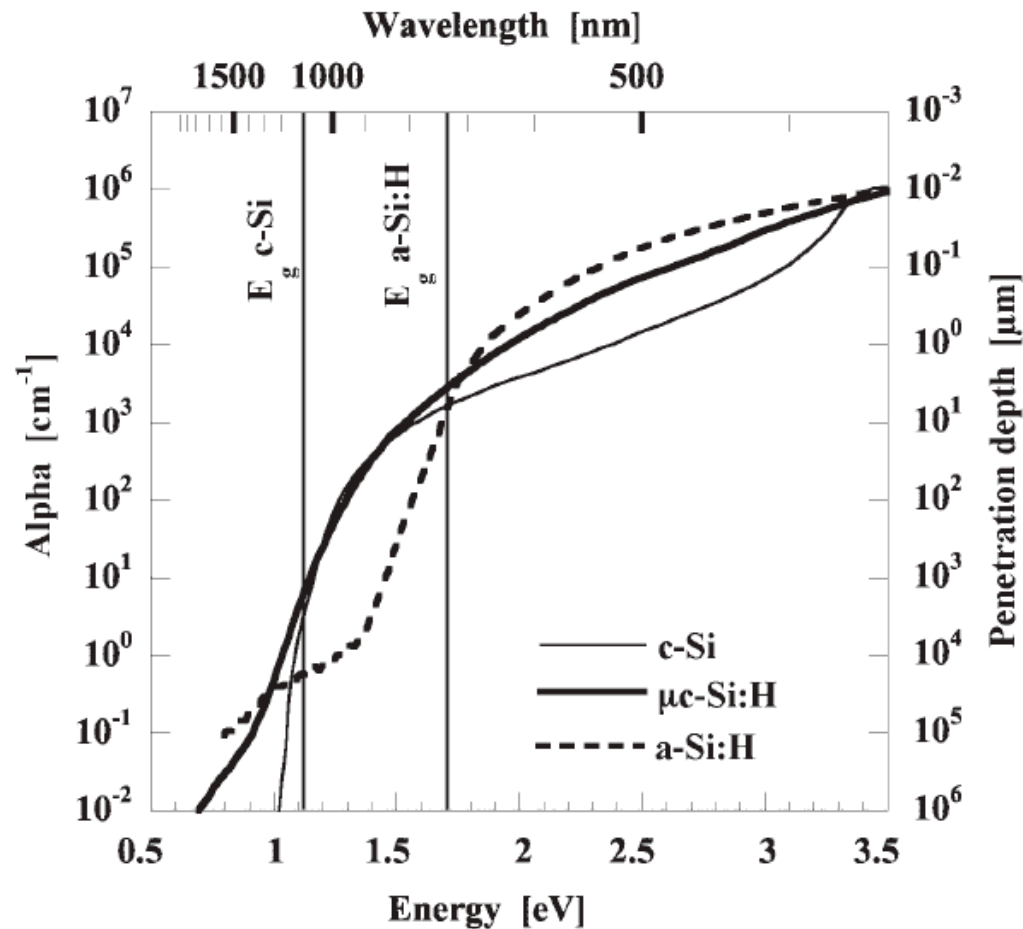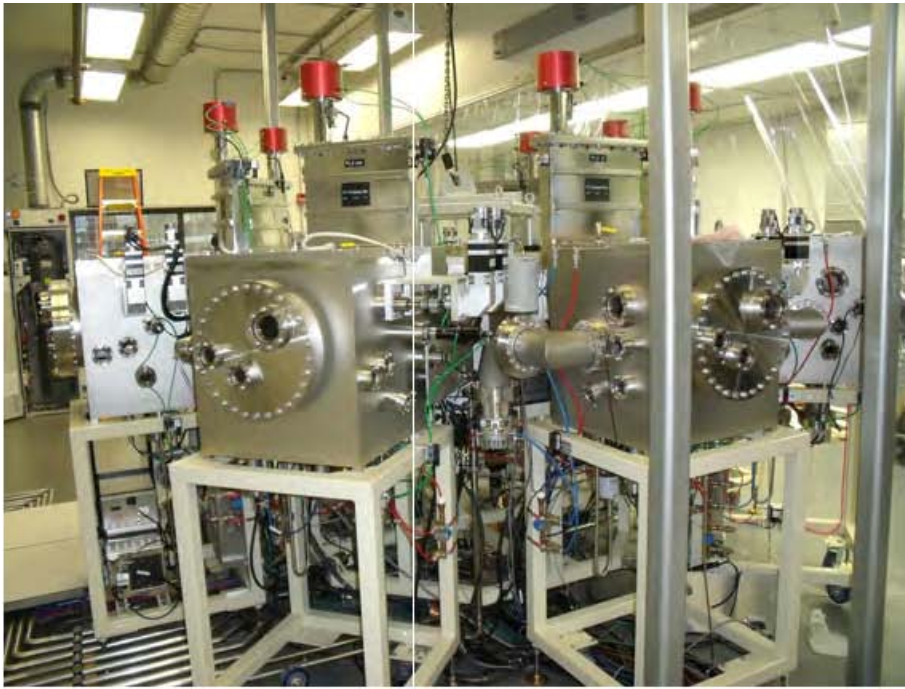

Figure 4. Curves for the optical absorption coefficient α and the penetration depth $d_\lambda = 1/\alpha$ of monochromatic light with photon energy $h\nu$ and wavelength λ, for wafer-type crystalline silicon (c-Si) and typical device-quality a-Si:H and μc-Si:H layers on glass.[15,16] The curve for μc-Si:H has been corrected for light scattering due to surface roughness[16]

- a-Si:H is typically deposited by plasma decomposition of SiH4, with other gases added for doping and alloying.
- Silane decomposes spontaneously at temperatures above ~450°C, forming polycrystalline or epitaxial silicon.
- Amorphous films can result at T < 550 °C, but films are typically of low quality because hydrogen is not retained.
- The deposition of a-Si:H requires a source of energy to dissociate the silane molecule.
- The first plasma deposition system for amorphous silicon was developed by Chittick *et al. (1969).*
- Most reactors are designed in a diode configuration where the plasma is confined between two parallel electrodes.
- Deposition usually lakes place at a gas pressure of 0.1- 1 Torr, which is the optimum pressure to sustain the plasma.
- Amorphous Si can be deposited by a variety of methods, but PECVD (aka RF plasma, or glow-discharge deposition) is the most common

Fig. 2.1. Schematic diagram of a typical rf diode plasma reactor for depositing a-Si:H and alloys.
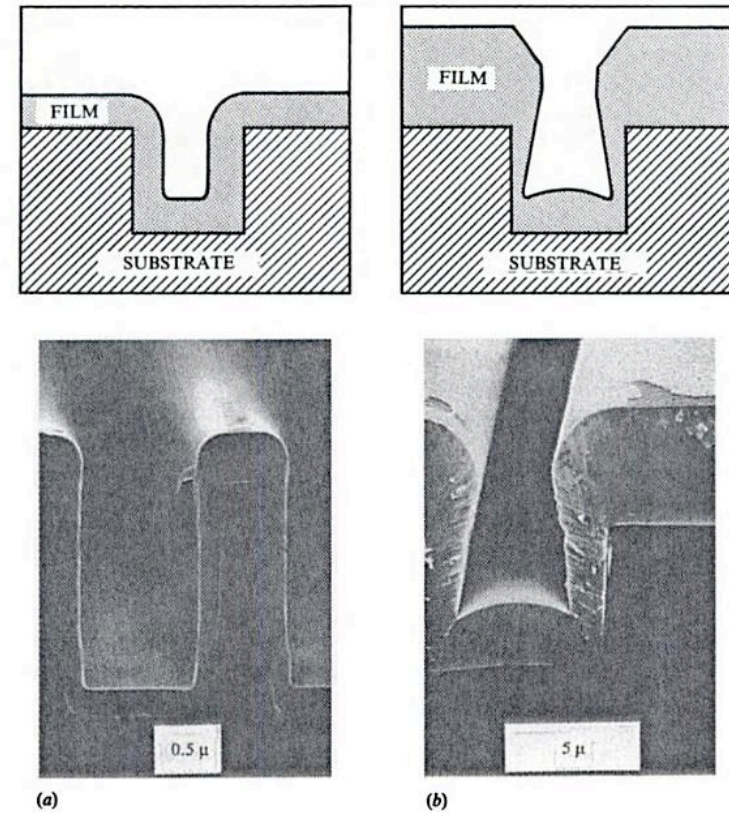
"Hydrogenated Amorphous Silicon" By R. A. Street
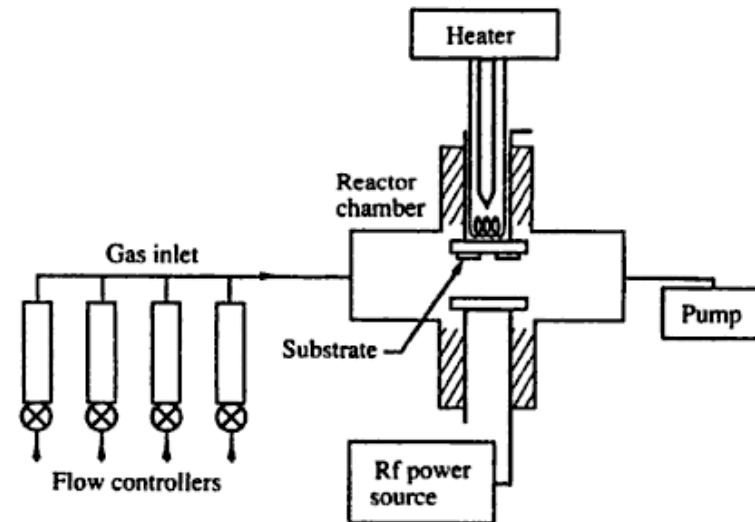
PECVC is Conformal, PVD (reactive sputtering) is more "line-of-site"

Fig. 2.7. Predicted (upper) and observed (lower) growth morphology of deposits made over a trench cut in a substrate, showing the difference between (a) CVD and (b) PVD growth processes (Tsai et al. 1986a).

Other methods:
Hot-wire CVD
Liquid source pyrolysis
......

"Hydrogenated Amorphous Silicon" By R. A. Street

Crystalline Si

1.1 eV indirect bandgap

4-fold coordination

fixed bond length and angles

long range order

1000 cm2/Vs

a-Si:H

1.7 – 1.9 eV direct bandgap

≤ 4-fold coordination; 3-fold most common

variable bond lengths and angles

short range order
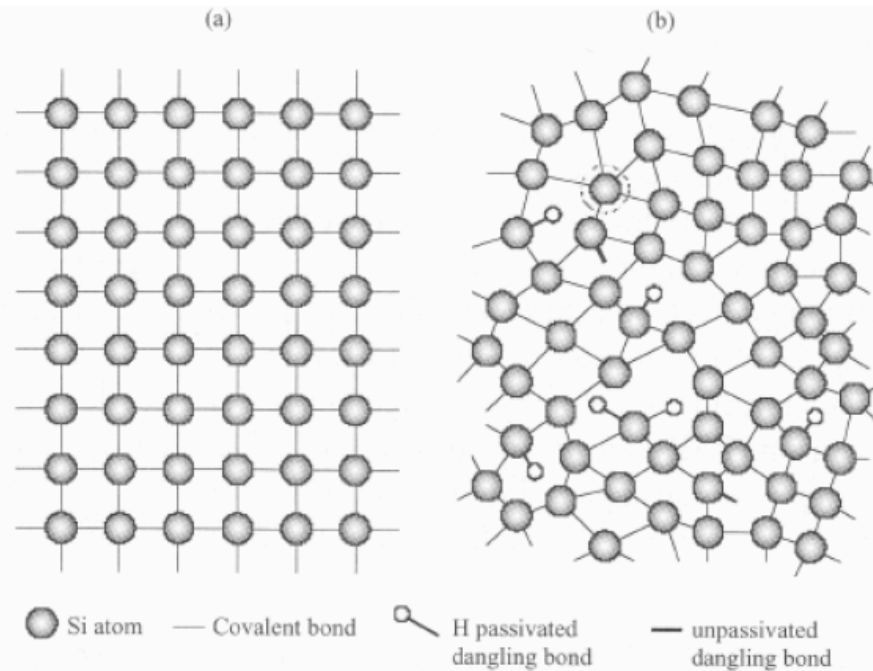
Low carrier mobility ~1 cm2/Vs

(a)   (b)

Si atom   — Covalent bond   H passivated dangling bond   — unpassivated dangling bond

Figure 5.1 Schematic representation of the atomic structure of (a) single crystal silicon, (b) hydrogenated amorphous silicon.

Thin Film Solar Cells, ed. J. Poortmans and V. Arkhipov (Wiley, 2006)
http://engphys.mcmaster.ca/undergraduate/outlines/4x03/Lecture%2016-17,%20a-Si.pdf

Energetically, a large number of ways that dopants can be included

Larger defect density in doped a-Si:H
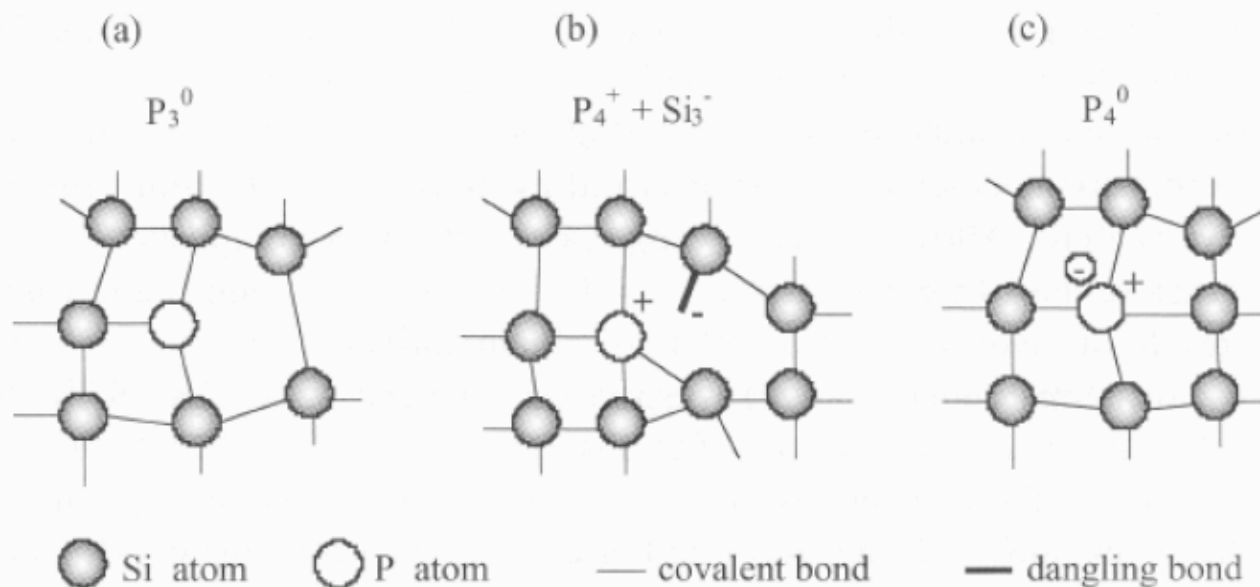Absorber layer must be intrinsic a-Si:H
Requires p-i-n structure

(a) P_3^0 (b) $P_4^+ + Si_3^-$ (c) P_4^0

● Si atom   ○ P atom   — covalent bond   — dangling bond

Figure 5.8 Possible configurations of a phosphorous atom in an a-Si:H network: (a) the nondoping state P_3^0, (b) the defect compensated donor state $P_4^+ + Si_3^-$, (c) the neutral donor P_4^0.

10^{21} cm^{-3} defects in pure a-Si

Defects are amphoteric, making doping difficult

Hydrogen in plasma passivates dangling bonds

e.g., H2 mixed with SiH4 in RF PECVD

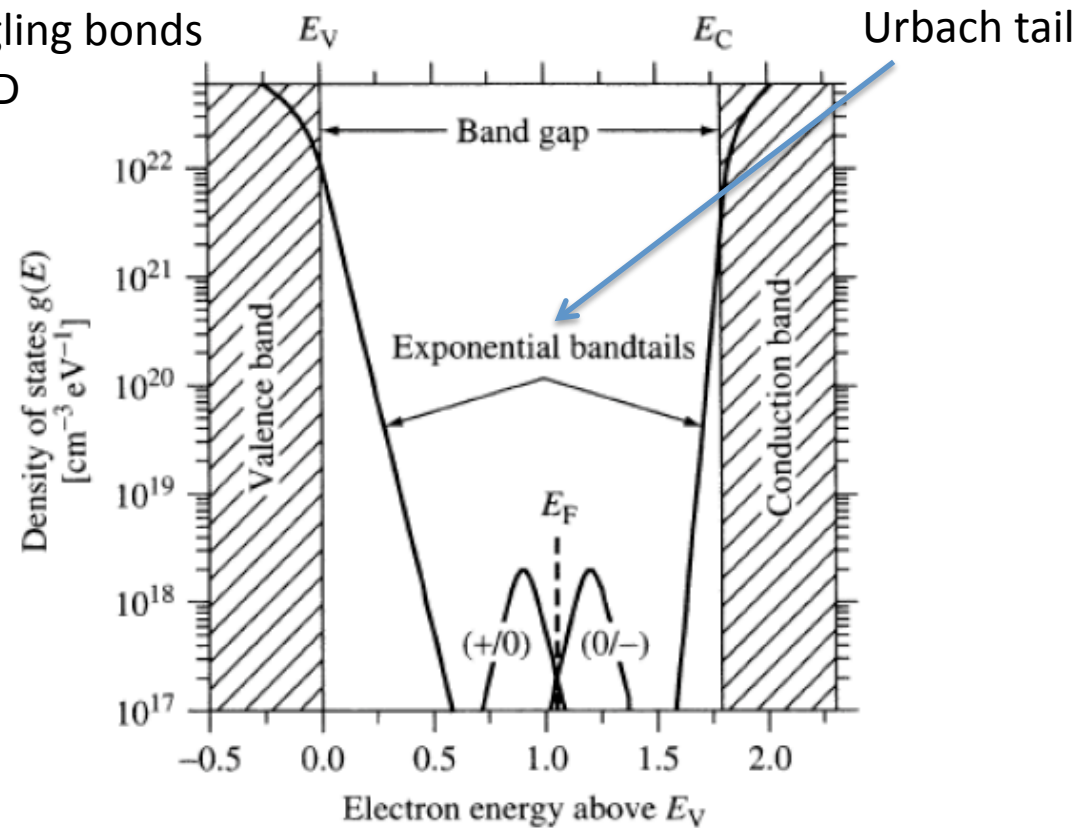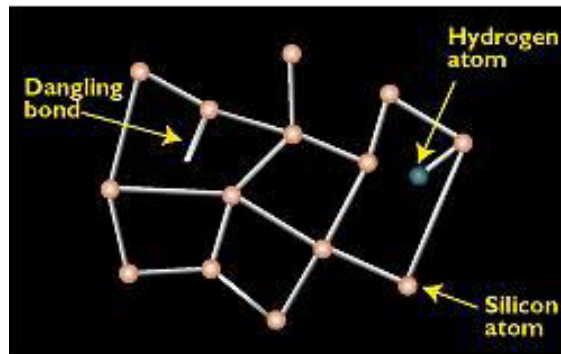< 10% H → $10^{15} - 10^{16}$ cm^{-3} defects

Urbach tail

Figure 12.9 Density of electronic states $g(E)$ in hydrogenated amorphous silicon. The shaded areas indicate delocalized states in the bands; these bands themselves have tails of localized states with an exponential distribution. Midway between the bands are levels belonging to gross defects such as dangling Si bonds indicated by the two peaked bands around E_F

F. Urbach, Phys. Rev. **92**, 1324 (1953).

Thin Film Solar Cells, ed. J. Poortmans and V. Arkhipov (Wiley, 2006)

http://engphys.mcmaster.ca/undergraduate/outlines/4x03/Lecture%2016-17,%20a-Si.pdf

R. Chittick accidentally obtained a-Si:H layers in a remote part of his plasma reactor. W. E. Spear and co-workers at Dundee University published the first systematic study on plasma-enhanced chemical vapor deposition (PECVD) with silane plus (optional) doping gases (1976). The figure shows schematically the results obtained by by plotting the values of dark conductivity and dark conductivity activation energy E_σ against gas doping ratio. Also plotted is the Fermi level (E_f) obtained by taking the E_σ values and correcting for the so-called statistical shift.
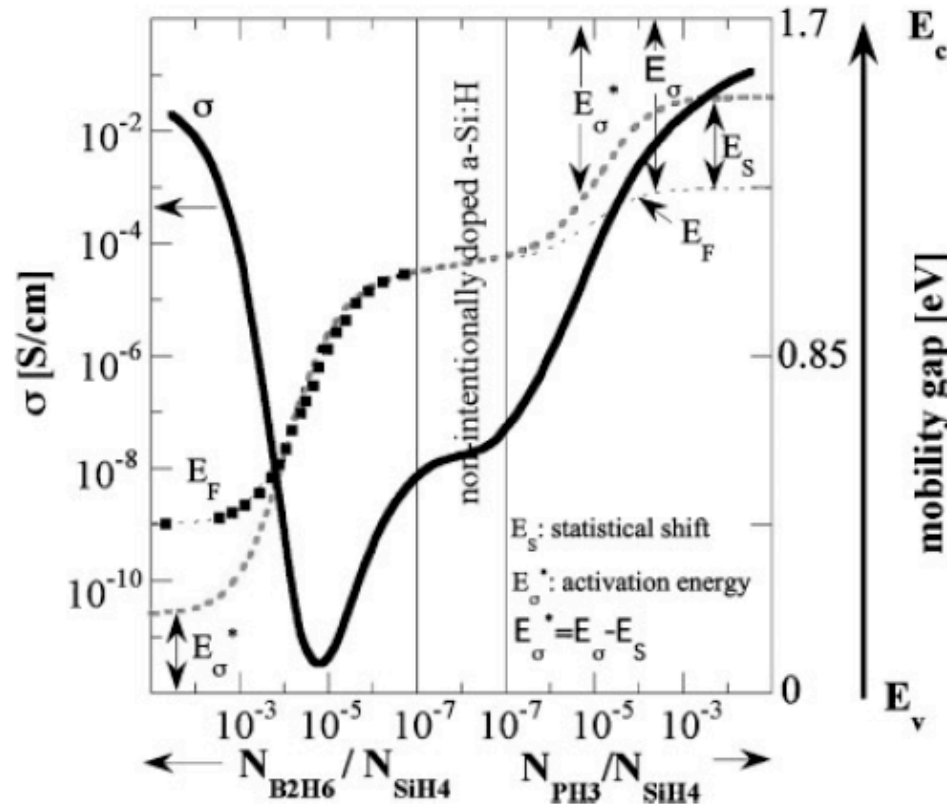

Figure caption: Dark conductivity (σ), activation energy E_σ of dark conductivity, and estimated position of Fermi level (E_f) for a-Si:H layers, produced by PECVD on glass, as a function of gas phase doping ratio NPH3/NSiH4 (for n-type layers) and NB2H6/NSiH4 (for p-type layers). Values of σ and E_σ are from Spear et al. E_σ* is here the estimated 'true' distance between band edge (Ec, Ev) and the Fermi level E_f, where the statistical shift E_s has additionally been taken into consideration for n- and p-type layers according to Overhof and Thomas (1989) assuming a constant defect density of $10^{16}/cm^2$ eV. The equivalent bandgap of a-Si:H, or the 'mobility gap' as it is called here, is taken to be 1.7 eV, while drawing the graph; this corresponds to the generally published values

After Shah, et al., "Thin-film Silicon Solar Cell Technology", Prog. Photovolt: Res. Appl. 2004;
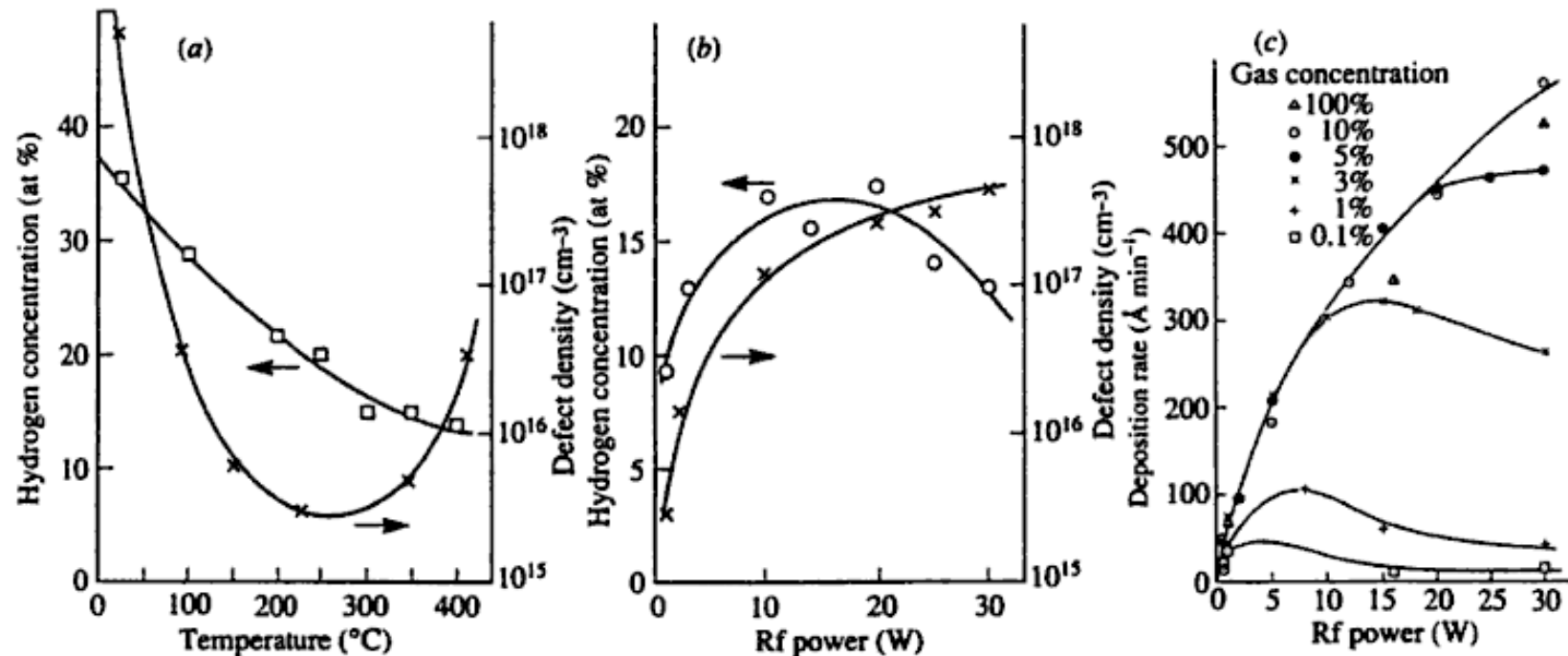
Characteristics of PECVD films grown from Silane

Fig. 2.2. Illustration of the dependence of material properties on deposition conditions, showing variations of the hydrogen concentration and defect density on (a) substrate temperature, and (b) rf power (Knights and Lucovsky 1980); (c) shows the dependence of the growth rate on power and argon dilution (Street, Knights and Biegelsen 1978).

"Hydrogenated Amorphous Silicon" By R. A. Street

Consequences of Disorder

Fig. 1.1. The correspondence between features of the atomi... the resulting electronic properties.

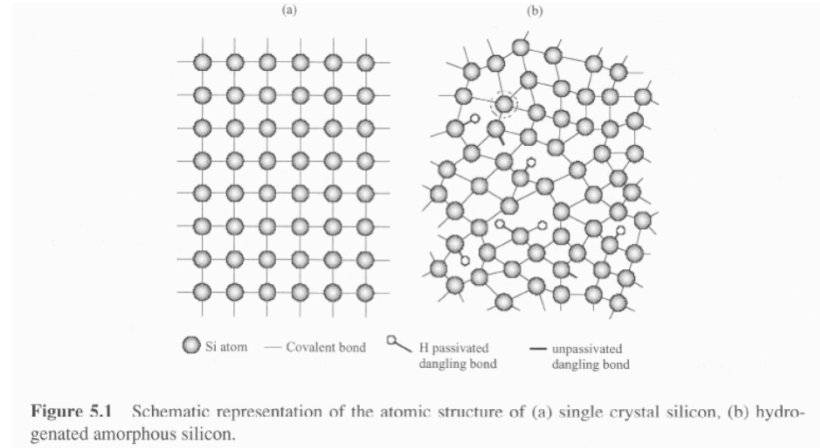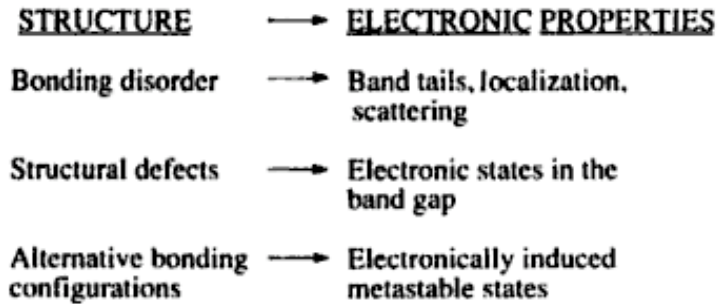STRUCTURE $\longrightarrow$ ELECTRONIC PROPERTIES

Bonding disorder $\longrightarrow$ Band tails, localization, scattering

Structural defects $\longrightarrow$ Electronic states in the band gap

Alternative bonding configurations $\longrightarrow$ Electronically induced metastable states

Si atom — Covalent bond — H passivated dangling bond — unpassivated dangling bond

Figure 5.1 Schematic representation of the atomic structure of (a) single crystal silicon, (b) hydrogenated amorphous silicon.

Fig. 1.9. The density of states distribution near the band edge of an amorphous semiconductor, showing the localized and extended states separated by the mobility edge.
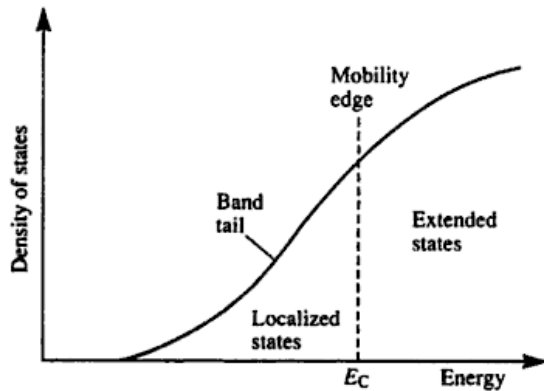

Fig. 1.6. Schematic density of states distribution for an amorphous semiconductor showing the bands, the band tails, and the defect states in the band gap. The dashed curves are the equivalent density of states in a crystal.
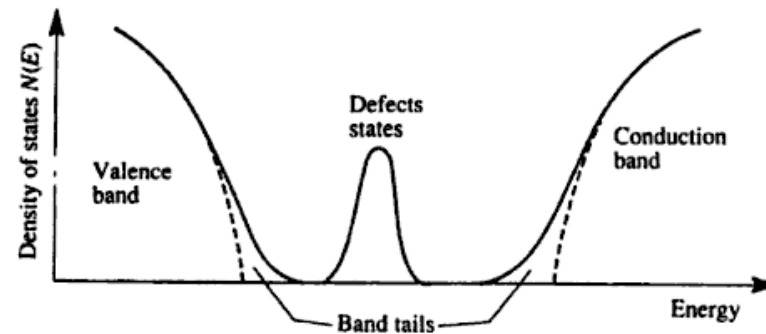

"Hydrogenated Amorphous Silicon" By R. A. Street

Fig. 1.8. The Anderson model of the potential wells for (a) a crystalline lattice and (b) an amorphous network. V_0 is the disorder potential.
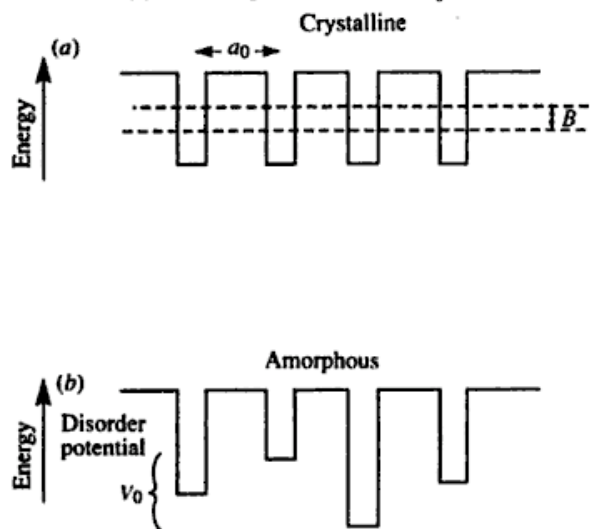
Crystalline

(a)

Energy

a_0

B
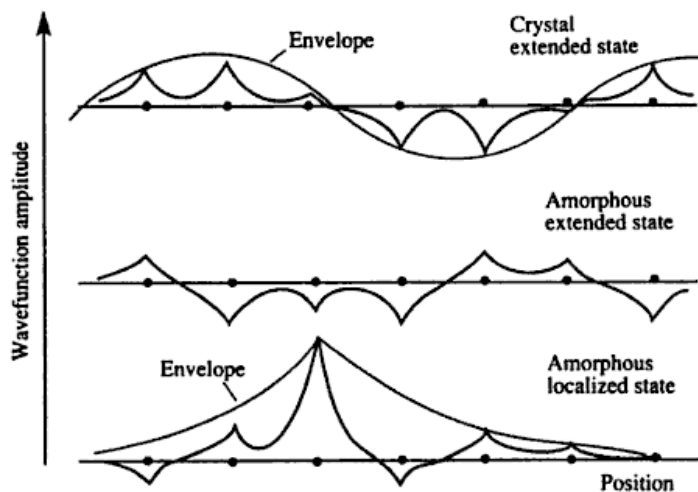
Amorphous

(b)

Energy

Disorder potential

V_0

Fig. 1.2. Schematic diagram of the atom pair distribution functions for a crystalline and amorphous solid and a gas, scaled to the average separation of nearest neighbor atoms, R_{av}, showing the different degree of structural order.
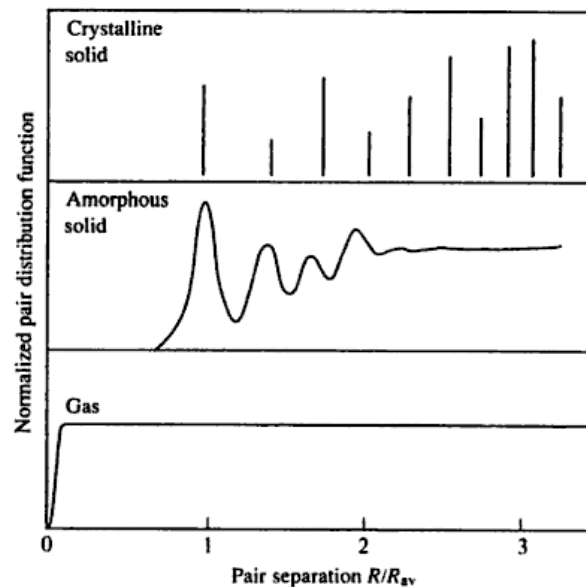
Normalized pair distribution function

Crystalline solid

Amorphous solid

Gas

0   1   2   3

Pair separation R/R_{av}

Fig. 1.7. Illustration of the wavefunctions of extended and localized states of an amorphous material, compared to the extended states of a crystal.

Wavefunction amplitude

Envelope

Crystal extended state

Amorphous extended state

Envelope

Amorphous localized state

Position

Fig. 1.10. Model showing the tunneling between two localized states separated by distance R and energy E_{12}; R_0 is the localization length.

R_0

②

E_{12}

①

R

"Hydrogenated Amorphous Silicon" By R. A. Street
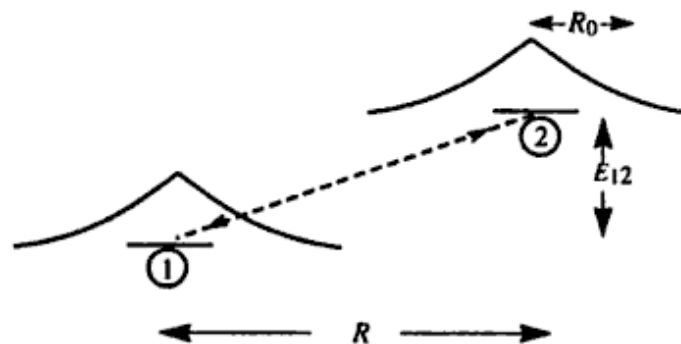
Various Si-H Species, and the growing interface

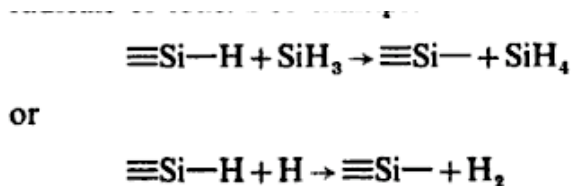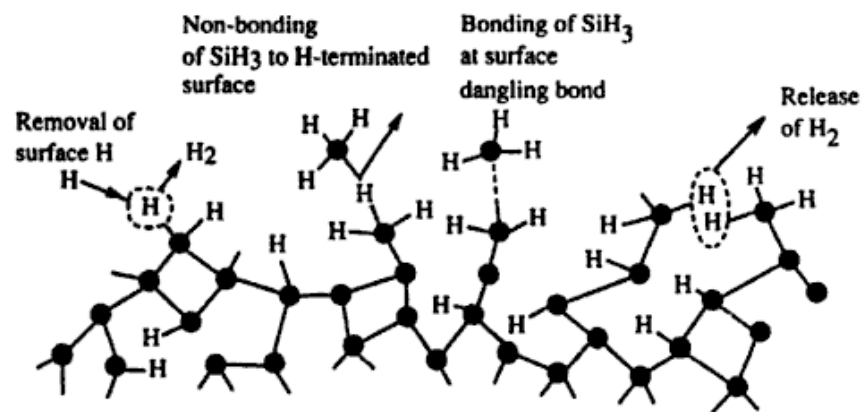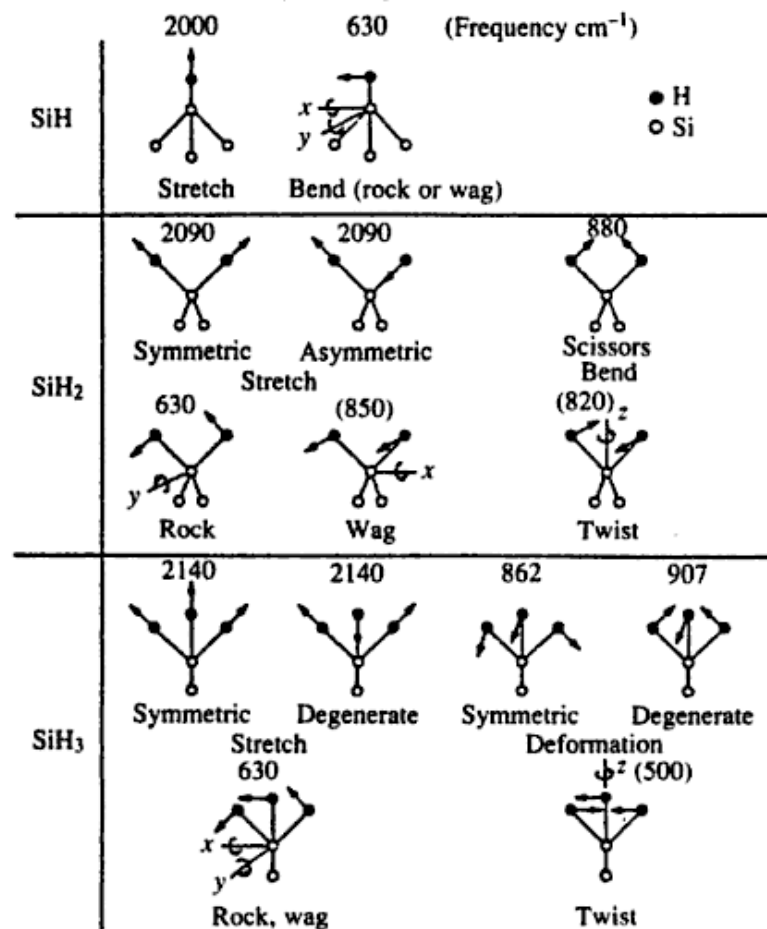Fig. 2.10. Illustration of some possible processes taking place at the a-Si:H surface during growth.

$$\equiv Si-H + SiH_3 \rightarrow \equiv Si- + SiH_4$$

or

$$\equiv Si-H + H \rightarrow \equiv Si- + H_2$$

Fig. 2.17. The set of Si—H vibrational modes for SiH, SiH$_2$ and SiH$_3$ groups, with calculated frequencies as indicated. The frequencies in brackets are estimates (Lucovsky et al. 1979).

"Hydrogenated Amorphous Silicon" By R. A. Street

Hydrogen dilution of silane can be used to control the material during growth. A high concentration of hydrogen causes the deposited films to become crystalline rather than amorphous. The crystallite size is small, often less than 100 Å, so the material is called *microcrystalline* silicon. The *power-dilution diagram for hydrogen*, below, shows the transition to microcrystallinity. Dilution to about *5 %* silane is needed to cause crystallization and the effect is enhanced by bigh rf power. The transition is fairly abrupt, and a mixed phase material is only observed in a narrow region near the dividing line.
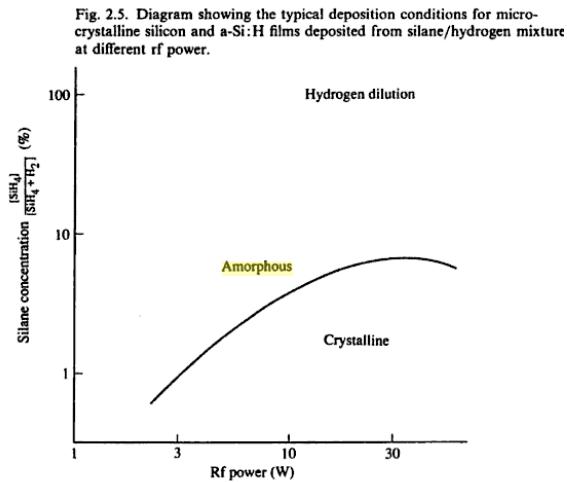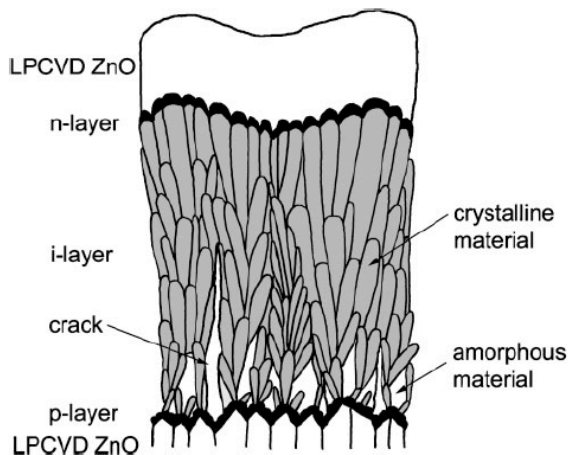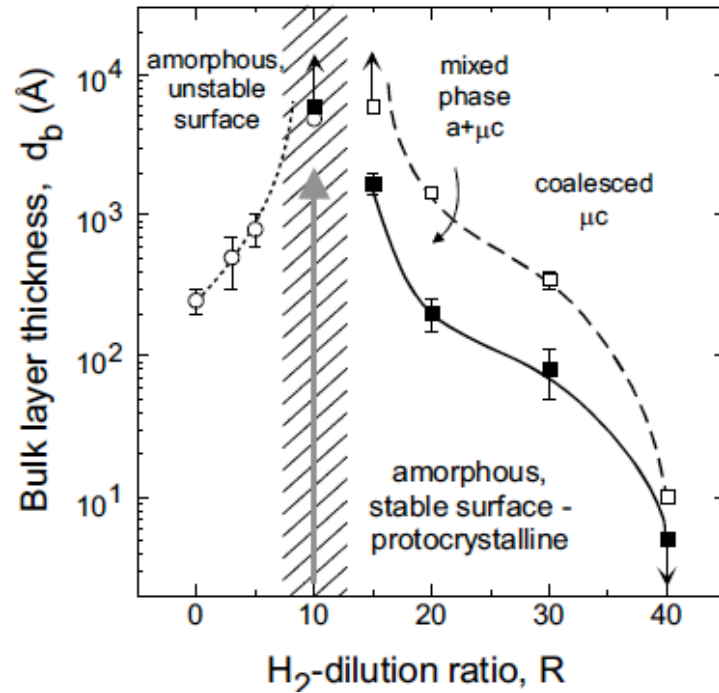

Fig. 2.5. Diagram showing the typical deposition conditions for micro-crystalline silicon and a-Si:H films deposited from silane/hydrogen mixture at different rf power.

Fig. 2.6. Illustration of (a) the shadowing effect of atoms on the growth surface, and (b) the resulting chain-like growth morphology when the sticking coefficient is high.

Wronski, et al., Proceedings of *RIO 02 - World Climate & Energy Event, January 6-11, 2002*

After Shah, et al., "Thin-film Silicon Solar CellTechnology", Prog. Photovolt: Res. Appl. 2004;

"Hydrogenated Amorphous Silicon" By R. A. Street

- The doping is not as straightforward in a-Si:H; E_f can be pushed only half way towards the conduction and valence band edges even with heavy doping.
- Doping has a detrimental effect on a-Si:H layer quality, because it leads to the many silicon dangling bonds (recombination centers).
- In a p/n crystalline solar cell, carrier collection is by minority carrier diffusion within the p- and n-layers. Long diffusion lengths (> 200 µm) assist carrier collection over the whole useful range of the solar cell thickness where significant optical absorption takes place.
- In a-Si:H layers, on the other hand, minority carrier diffusion lengths are extremely small (around 0.1 µm), and the device cannot rely on collection of photogenerated carriers by diffusion alone.
- The p–i–n structure builds a field into the device, and the field is distributed across the intrinsic (i) portion of the device.
- The intrinsic portion of the device typically has the best characteristics for absorption, photogeneration, and carrier lifetime, as compared to the p- and n-type regions
- The p–i–n-type a-Si:H cell was introduced by Carlson and Wronski in 1976.

Amorphous silicon solar cell

D. E. Carlson and C. R. Wronski

RCA Laboratories, Princeton, New Jersey 08540
(Received 6 February 1976)

Thin film solar cells, ~1 μm thick, have been fabricated from amorphous silicon deposited from a glow discharge in silane. The cells were made in a *p-i-n* structure by using doping gases in the discharge. The best power conversion efficiency to date is 2.4% in AM-1 sunlight. The maximum efficiency of thin-film amorphous silicon solar cells is estimated to be ~14–15%.
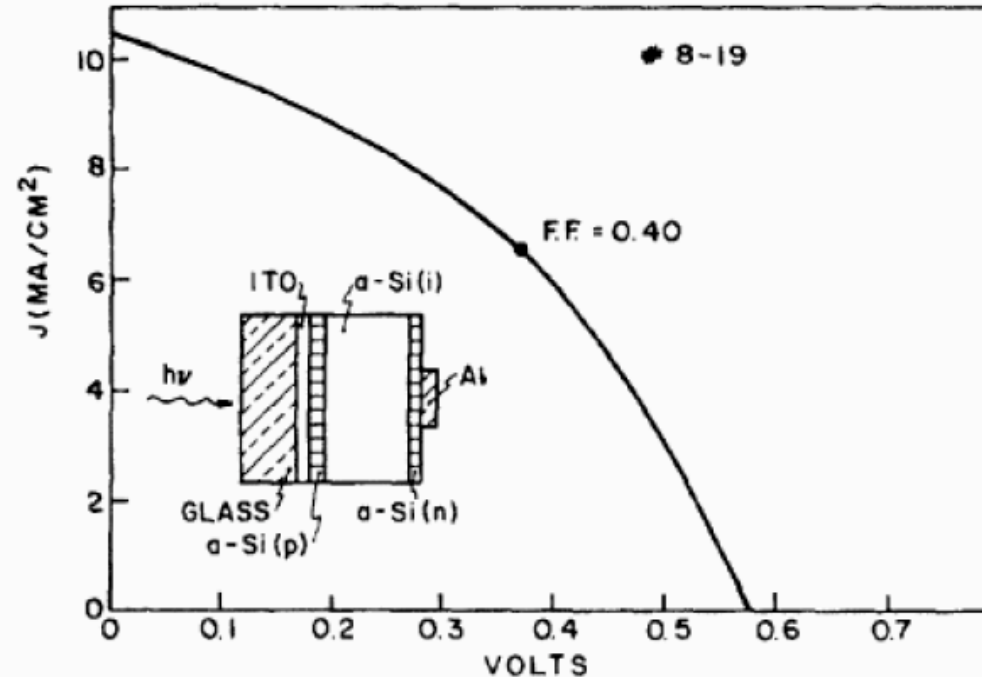
FIG. 1. Current–voltage curve for device #8–19 under illumination comparable to AM-1 sunlight. Also included in the figure is a schematic diagram of a *p-i-n* structure.

Superstrate configuration: Deposition on TCO coated glass

n- and p-regions are thin since minority carriers have low mobility
Most absorption occurs in thick *i* region, where carriers are collected by drift.
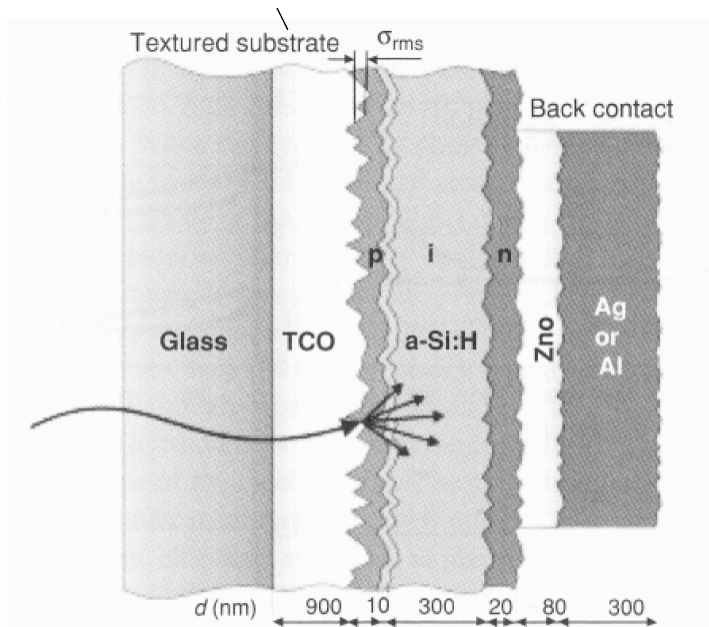Low doping in i-region to establish electric field (10^4 V/cm)

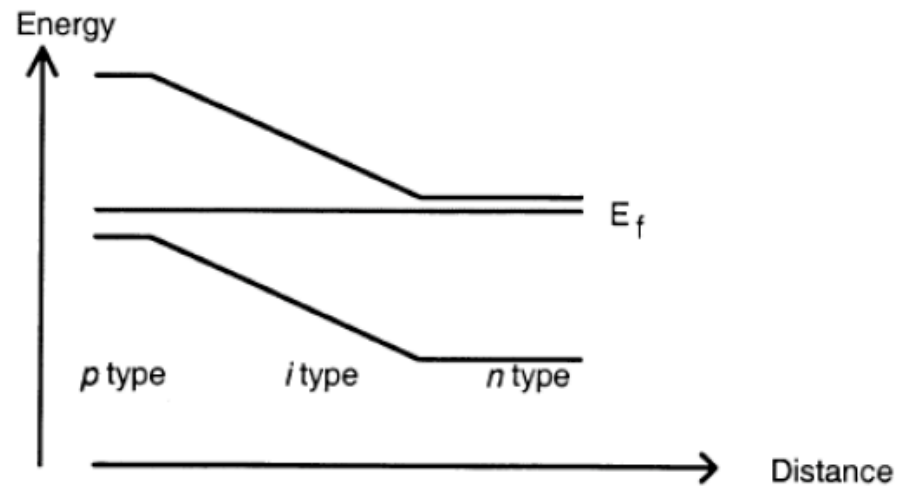**Figure 5.11**   A single junction p-i-n a-Si solar cell structure.

Fig. 8.8.   Band profile of $p–i–n$ junction.

Thin Film Solar Cells, ed. J. Poortmans and V. Arkhipov (Wiley, 2006)

The Physics of Solar Cells, J. Nelson, Imperial College Press, 2003

TCO is textured for light trapping,
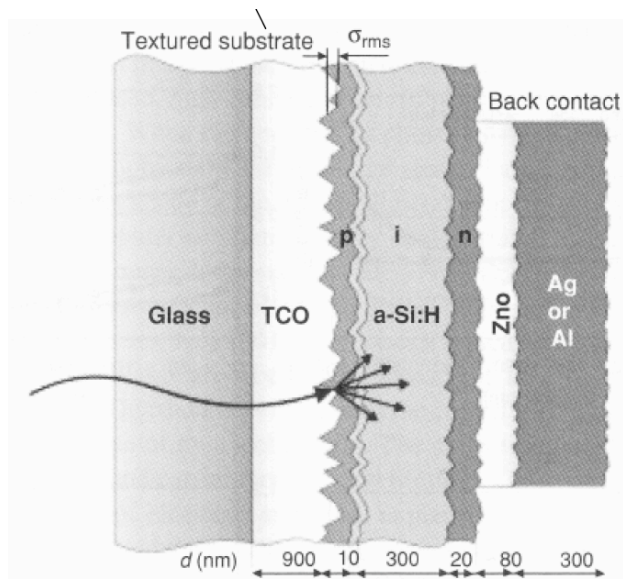relatively thick for high conductivity (often ITO)

Figure 5.11   A single junction p-i-n a-Si solar cell structure.

Table 5.2   Properties of several TCO front electrode films

Property	Requirement	ITO	SnO$_2$:F APCVD	ZnO:B LPCVD	ZnO:Al sputtering
Transmission (350–1000 nm)	>90 %	95 %	90 %	90 %	90–95 %
Bandgap [eV]	>3.5	3.7	4.3	3.4	≈3.45[a]
Sheet resistance [Ω/]	<10	3–5	6–15	6–15	4–15
Contact resistance to amorphous p$^+$ layer	low ohmic	low ohmic	low ohmic	forms barrier	forms barrier
Roughness	textured	negligible	excellent	excellent	excellent (after treatment)
Plasma durability	resistant	low	good	excellent	excellent

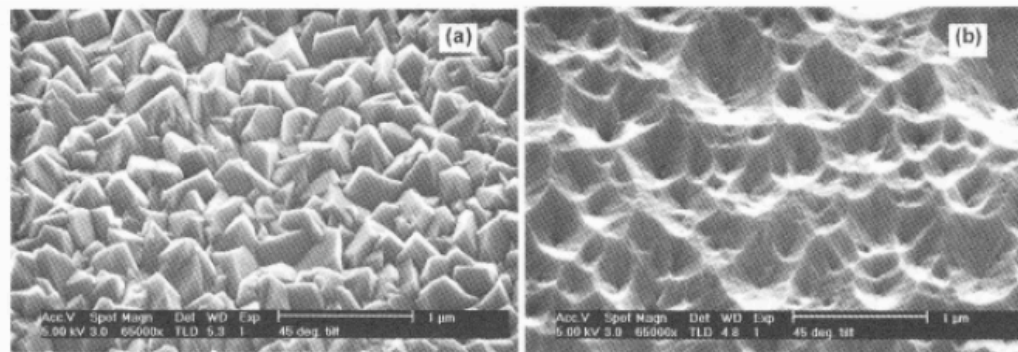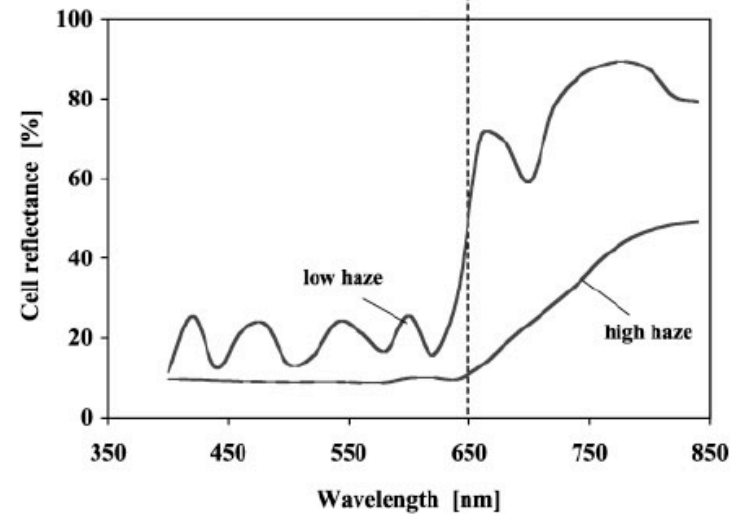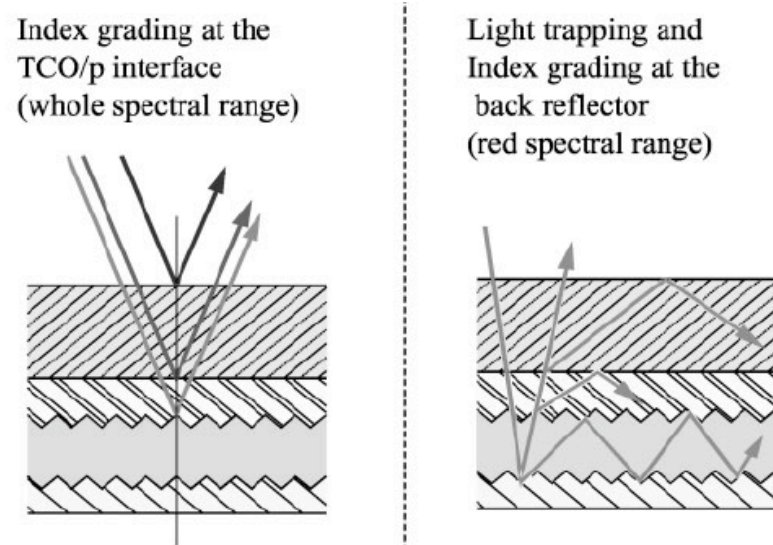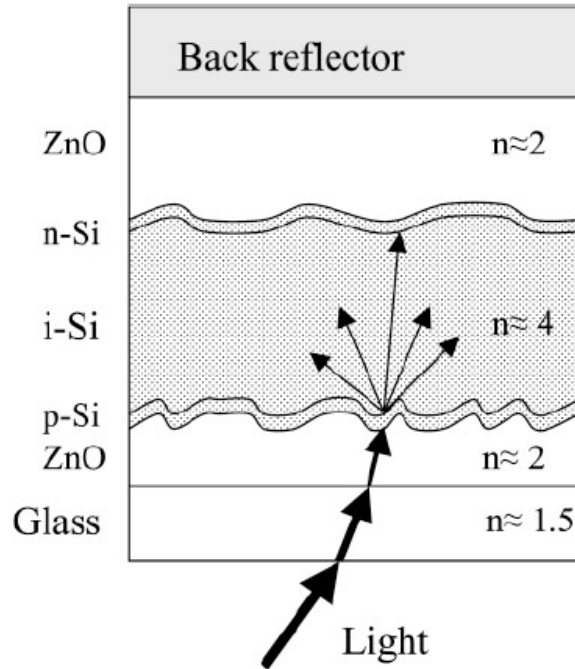[a] depends on electrical properties (mobility, carrier density, Burstein—Moss shift).

Figure 5.13   Scanning electron microscopy pictures of surface textured TCO substrates: (a) SnO$_2$:F Asahi U and (b) 10 s etched ZnO:Al TCO surface.

Thin Film Solar Cells, ed. J. Poortmans and V. Arkhipov (Wiley, 2006)

Importance of Light Trapping

Reflectances from cells with TCO of low and high haze, respectively. Measurement is performed with light incident from the glass side, in the glass/TCO/p–i–n/metal configuration

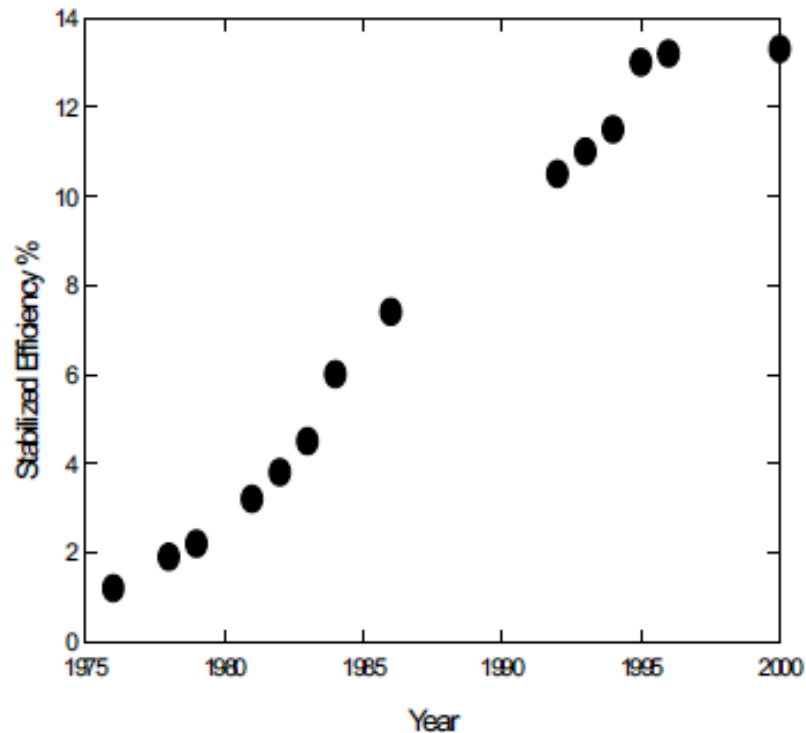# Steady growth in performance, but topped-out since 2000

Figure 1. Advances in Stabilized efficiency of a-Si:H solar cells.

Wronski, et al., Proceedings of *RIO 02 - World Climate & Energy Event, January 6-11, 2002*

Staebler-Wronski Effect

a-Si:H efficiency degrades ~30% under illumination over a time scale of months due to creation of additional dangling bond defects

Must distinguish between initial efficiency versus stabilized efficiency
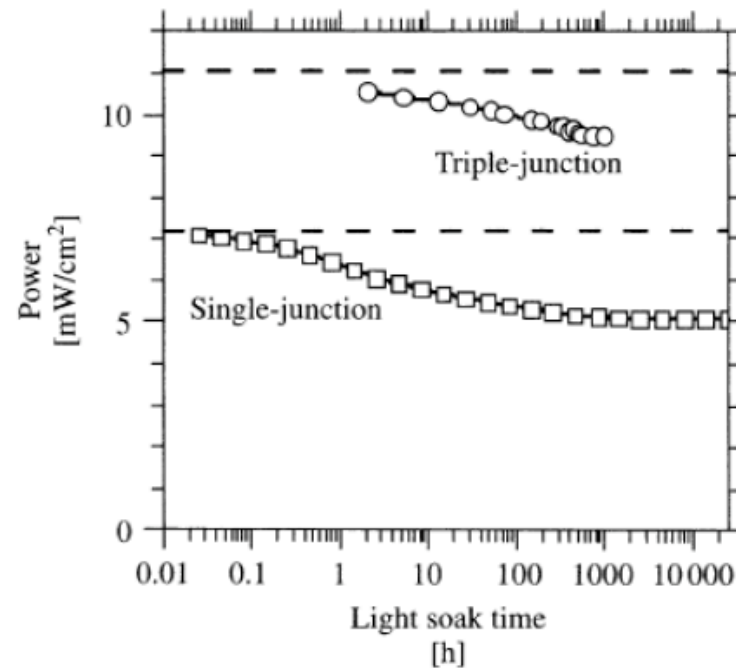

Figure 12.5 The conversion efficiency in a-Si:H-based solar cells declines noticeably upon the first exposure to sunlight. The figure illustrates this decline under a solar simulator (100 mW/cm²) for a single-junction cell (260-nm i-layer thickness) and for a triple-junction module made at United Solar Systems Corp. [14, 15]; the dashed lines indicate the initial power measured for each device

Thin Film Solar Cells, ed. J. Poortmans and V. Arkhipov (Wiley, 2006)

Staebler-Wronski Effect

Defects can be annealed out

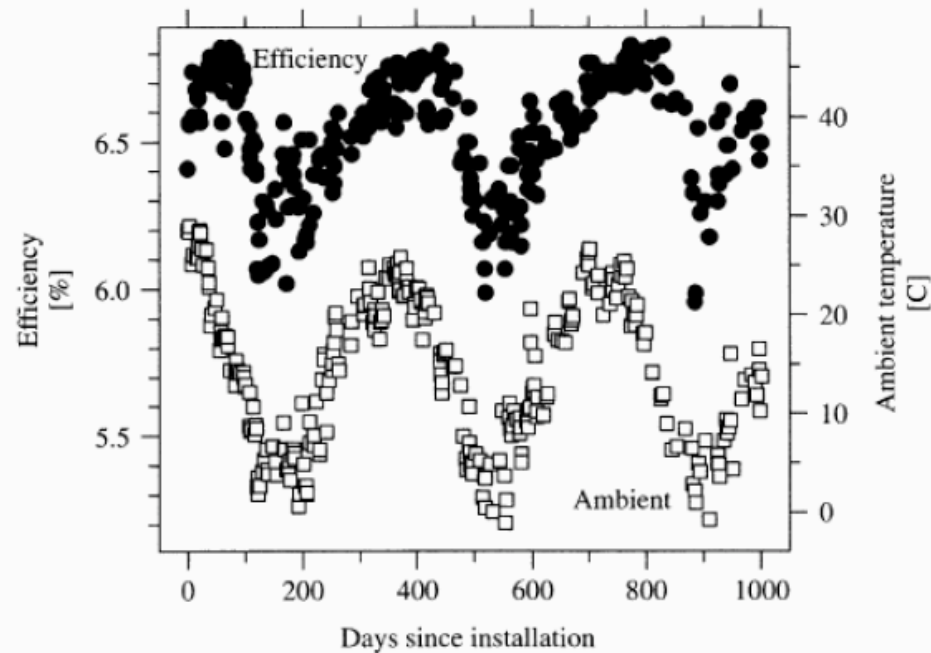Leads to seasonal efficiency variations

Figure 12.6 Seasonal variations in the average conversion efficiency (solid symbols) of an amorphous silicon triple-junction module [18], along with the daily mean temperature (open symbols

Thin Film Solar Cells, ed. J. Poortmans and V. Arkhipov (Wiley, 2006)

Multijunction Cells

Combine layers of different bandgaps to more efficiently convert different regions of the spectrum into carriers
Equivalent to placing cells in series
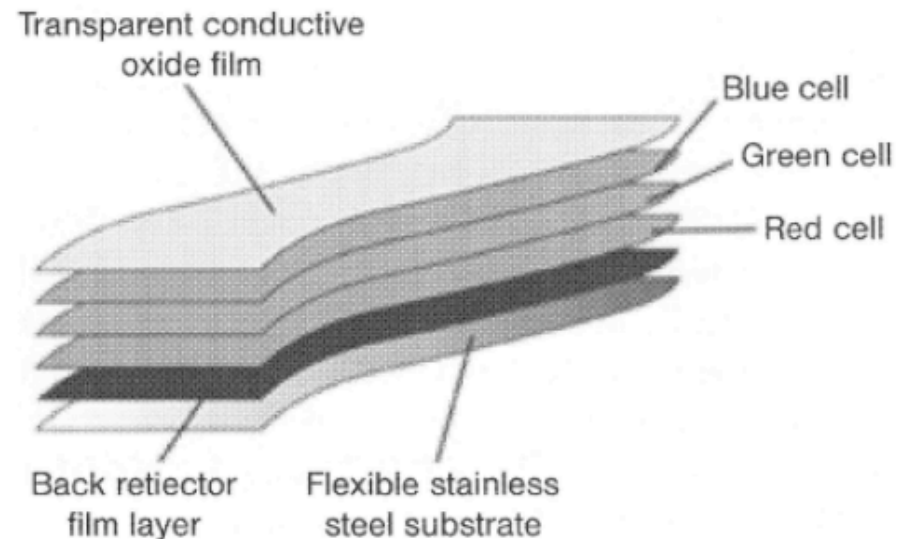Higher V_{oc} = sum of component cell V_{oc}'s
Higher efficiency

Figure 3.9 Amorphous silicon schematic of a triple-junction structure. (Reproduced from Uni-solar.com, with permission).

Alloys

Alloy with C   Methane, CH_4 in PECVD

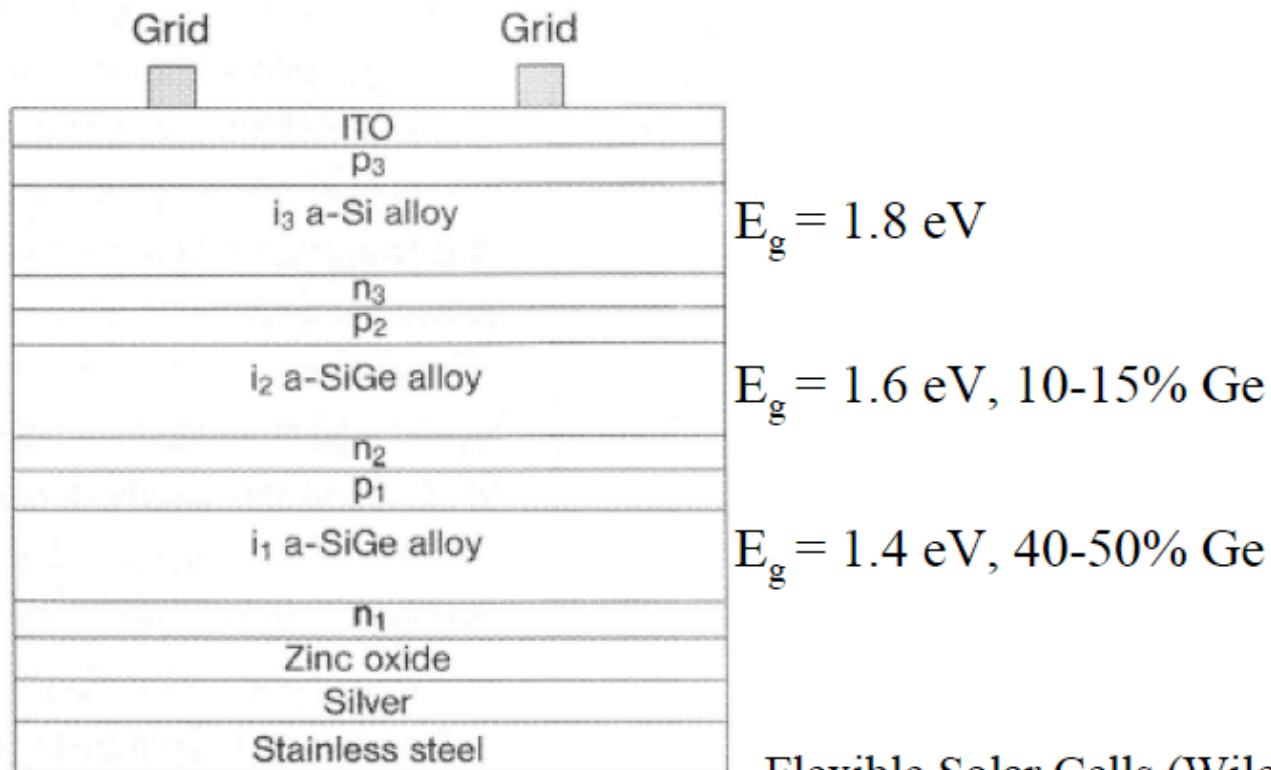Alloy with Ge   Germane, GeH_4 in PECVD

a-Si:H   Bandgap $1.7 - 1.8$ eV

$a\text{-}Si_{1-x}Ge_x\text{:}H$ Bandgap from 1.1 eV (x=1) to 1.7 eV (x=0)

a-SiC:H   Larger bandgap

Grid	Grid

| ITO |
| p_3 |
| i_3 a-Si alloy |
| n_3 |
| p_2 |
| i_2 a-SiGe alloy |
| n_2 |
| p_1 |
| i_1 a-SiGe alloy |
| n_1 |
| Zinc oxide |
| Silver |
| Stainless steel |

$E_g = 1.8$ eV

$E_g = 1.6$ eV, 10-15% Ge

$E_g = 1.4$ eV, 40-50% Ge

Flexible Solar Cells (Wiley, 2008)

Grid Grid

ITO
p_3
i_3 a-Si alloy

n_3
p_2
i_2 a-SiGe alloy

n_2
p_1
i_1 a-SiGe alloy

n_1
Zinc oxide
Silver
Stainless steel
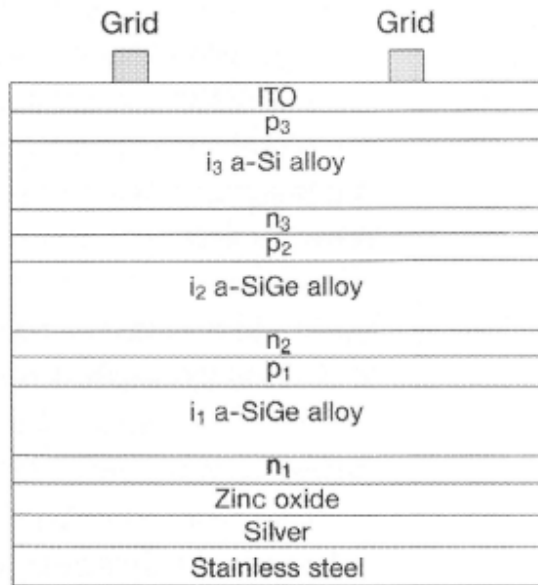
Currents at max. power point need to be matched for series connected cells

Using Tunnel junctions
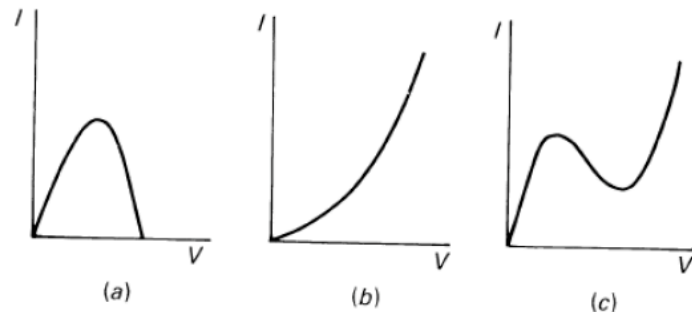
10 nm (20 atoms) thick layers over a meter wide !

p n

(a)   Conduction band
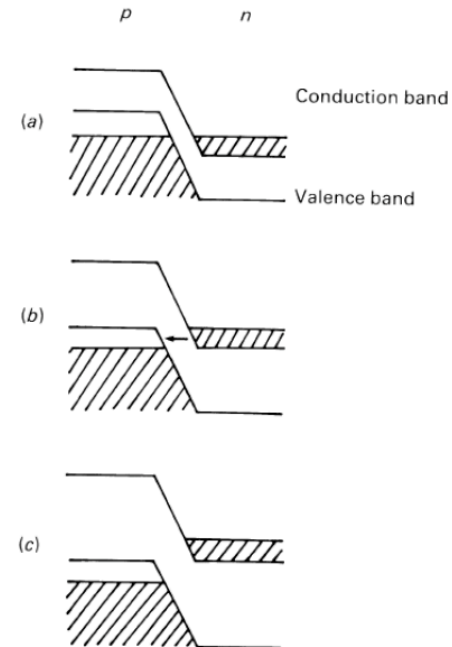
    Valence band

(b)

(c)

Figure 2.17. Tunnel diode energy level diagrams for different forward-bias voltages: (a) zero bias; (b) biased to the point of maximum tunneling current; (c) biased to the point where the tunneling current is again zero.

I I I

(a)   (b)   (c)
V   V   V

Figure 2.18. Forward-bias current components in the tunnel diode: (a) tunneling current; (b) diffusion current; (c) total current.

From Dunlap, "Experimental Physics", Oxford University Press, 1988

14.6% record stabilized efficiency (United Solar)

J_{sc} = 8.57 mA/cm^2

V_{oc} = 2.357 V

FF = 0.723

Eff = 14.6 %

A = 0.25 cm^2

Total
26.88
mA cm^{-2}
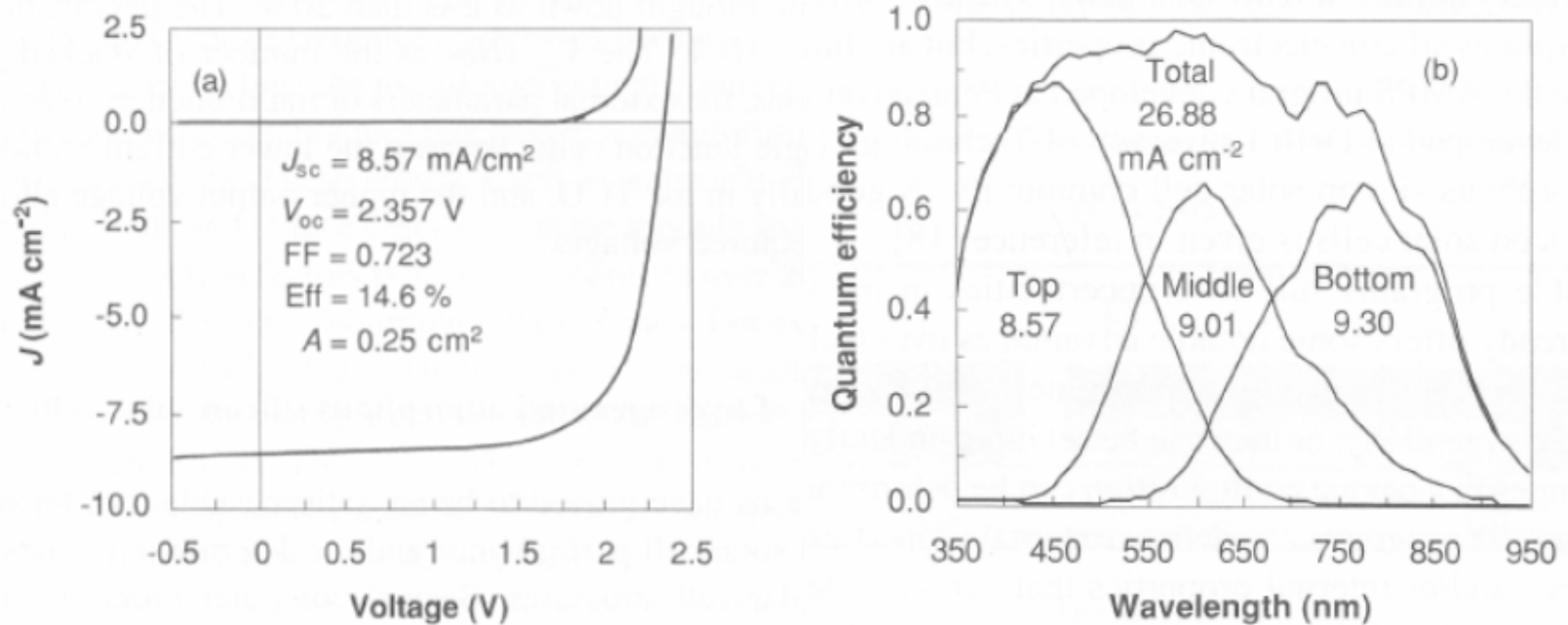
Top
8.57

Middle
9.01

Bottom
9.30

Figure 5.16 (a) Initial AM1.5 J-V characteristic and (b) quantum efficiency of an a-Si:H/a-SiGe:H/a-SiGe:H triple junction solar cell. (Courtesy of Jeff Yang, United Solar Ovonic Corporation).

Thin Film Solar Cells, ed. J. Poortmans and V. Arkhipov (Wiley, 2006)
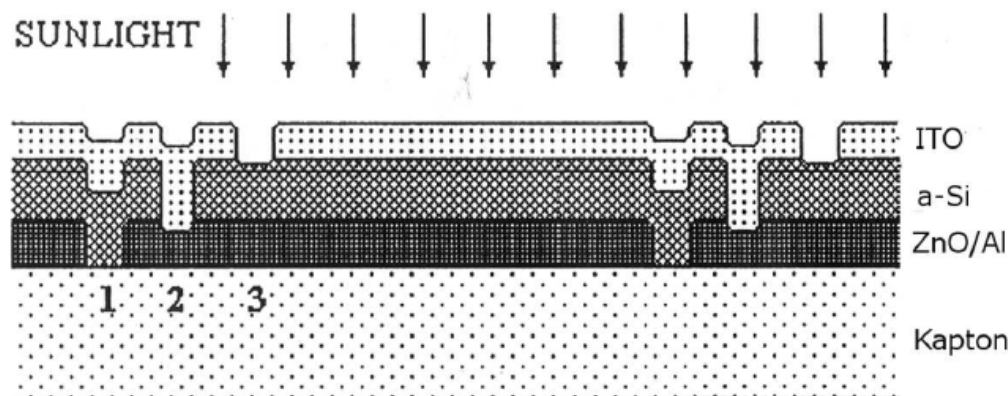
Figure 4-1: Three scribe scheme for series interconnection (adapted from [Comp00])

Simplest of all scribe approaches..
1. First scribe isolates strips of the back reflector (back contact): buffer and metal layers must be completely removed without damage to substrate. a-Si deposited after Scribe 1.
2. Second scribe is made to open a *via* in the amorphous silicon layers - all the amorphous silicon layers must be removed without damage to the back reflector layers. Then the TCO front contact (e.g. ITO) is deposited, covering entire front surface of the cell and penetrating the *vias* in the a-Si layers to make contact with the back reflector.
3. Third scribe then completes the interconnected cell by removal of the ITO layer without damage to the a-Si layer.

From "Triple Junction Amorphous Silicon based Flexible Photovoltaic Submodules on Polyimide Substrates", by Aarohi Vijh, 2005, The University of Toledo (thesis under supervision of Prof. Xunmeng Deng)

Series-connection holes
Current-collection holes

Unit cells

Transparent electrode

a-Si based layer

Metal electrode

Laser-scribing lines

Plastic film substrate
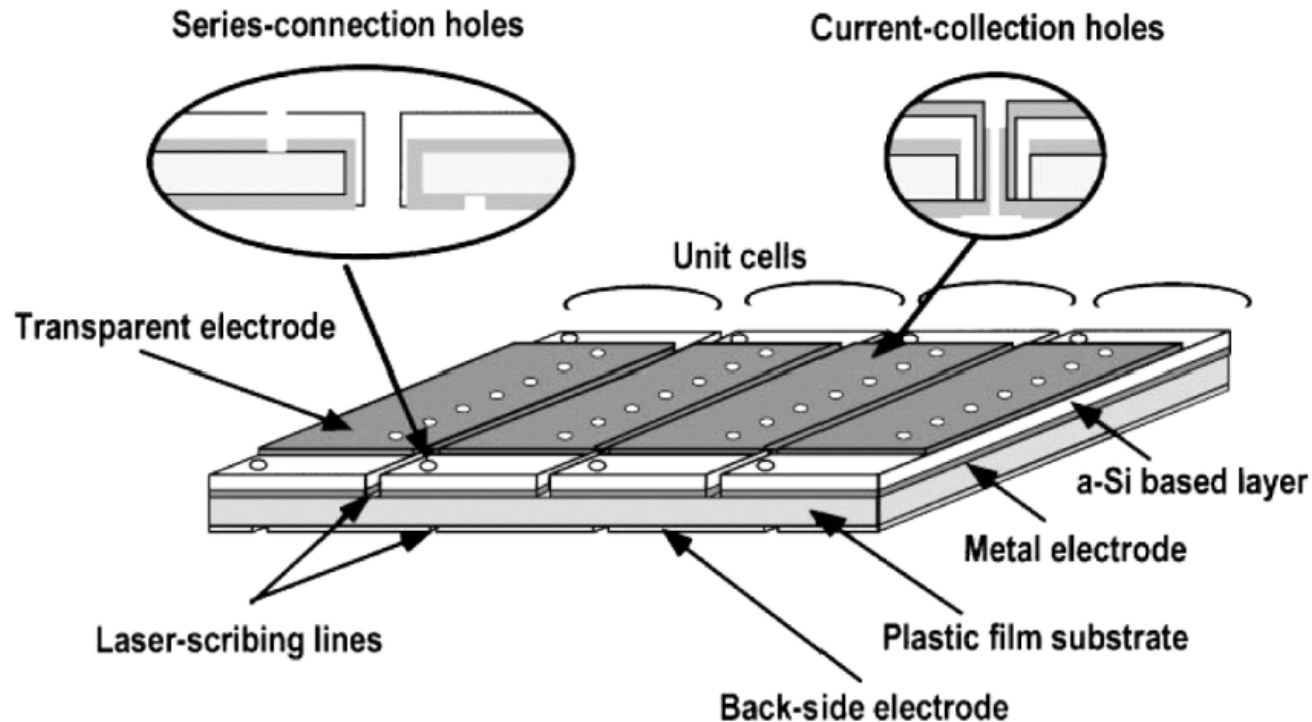
Back-side electrode

Figure 4-2: Fuji's SCAF interconnect scheme [Ichi01]

The "Fuji Electric" scheme uses sputtered metal contacts on both sides of a perforated plastic film – sputtering allows electrical connection of both sides through the perforations. After deposition of all films, laser scribing finishes the interconnection.
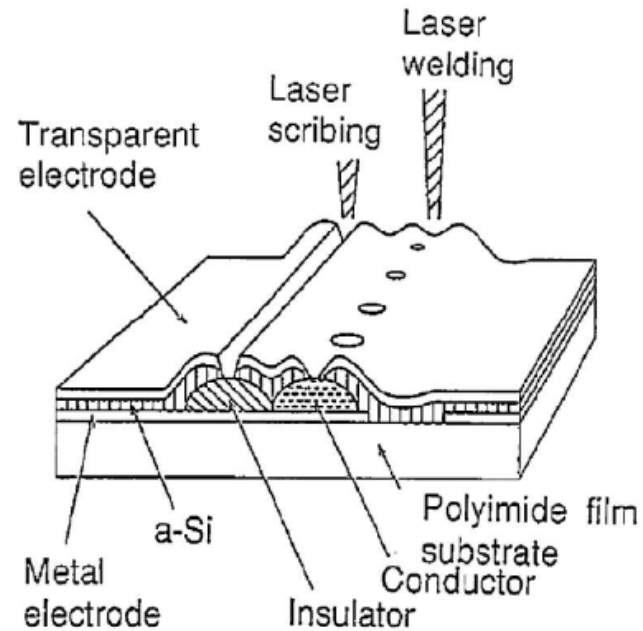
Figure 4-3: Sanyo's "'weld"' interconnect scheme [Nish95]

On this slide and next -- interconnection schemes used by Sanyo Electric and Iowa Thin Film Technologies (ITFT).

Similar to one another, they both use a line of insulating ink that acts as a laser beam stop – to prevent shunting of the cells during laser scribing of the ITO contact.

From "Triple Junction Amorphous Silicon based Flexible Photovoltaic Submodules on Polyimide Substrates", by Aarohi Vijh, 2005, The University of Toledo (thesis under supervision of Prof. Xunmeng Deng)
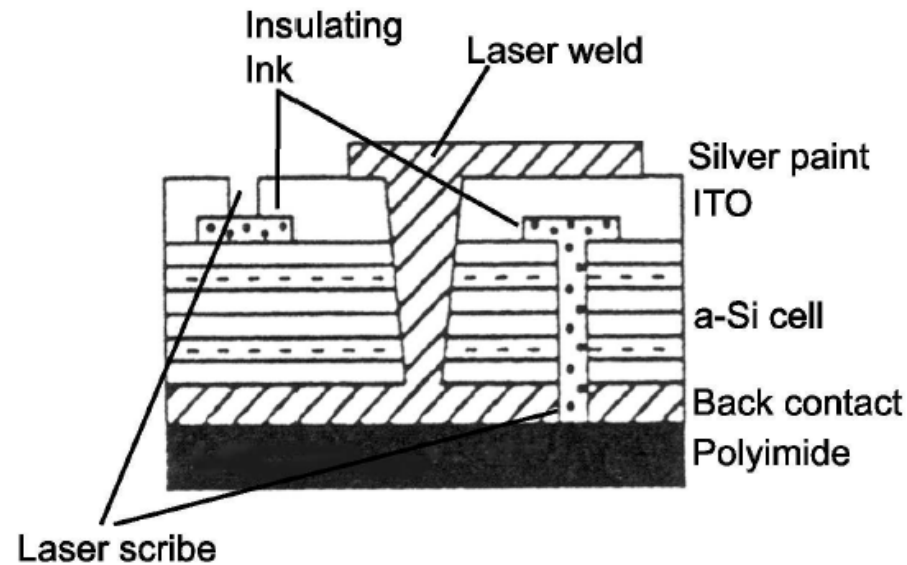
Figure 4-4: ITFT's laser-weld based interconnection scheme [Grim96].

Interconnection scheme used by Iowa Thin Film Technologies (ITFT).

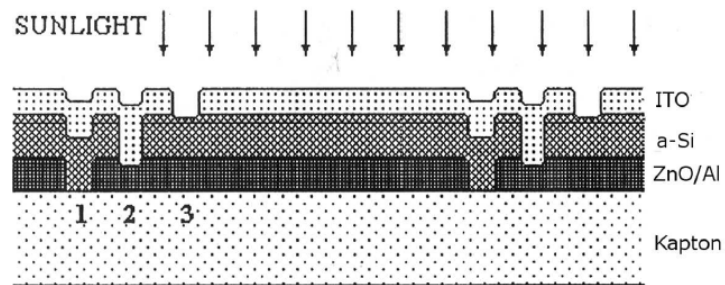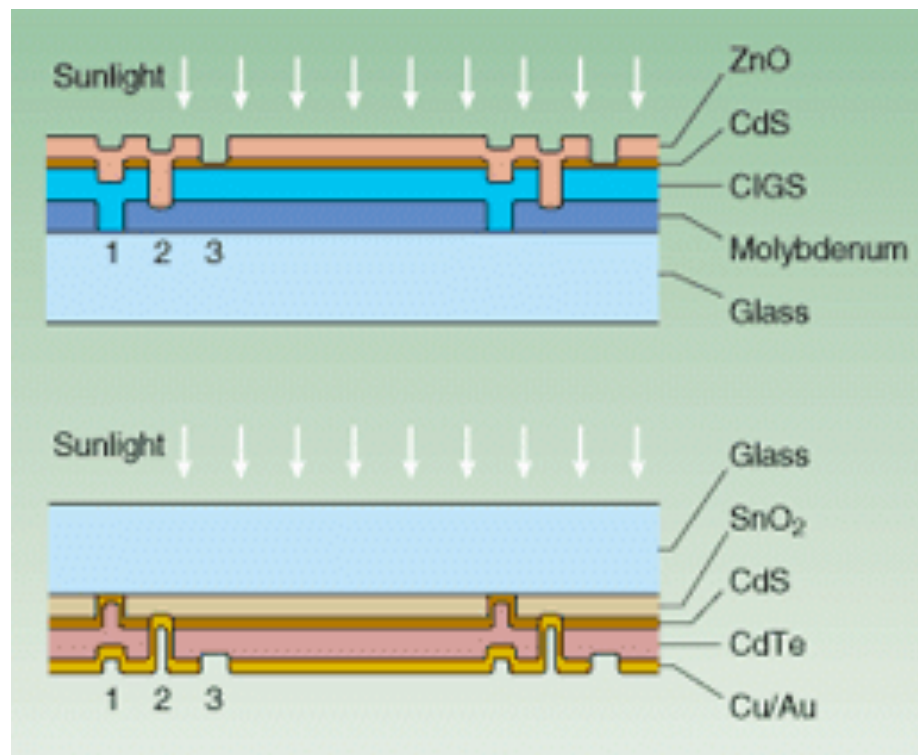# "Simple" a-Si scheme compared to monolithic integration of CdTe and CIGS devices

Figure 4-1: Three scribe scheme for series interconnection (adapted from [Comp00])

Substrate Configuration (suitable for flexible substrates, Roll-to-Roll)

e.g., United Solar, Xunlight

Xunlight Triple-Junction

Metal electrode

| TCO |
| p |
| i |
| n |
| TCO |
| Ag or Al reflector/electrode |
| stainless steel, or temp. resistant polymer (polyimid) |